

We are IntechOpen, the world's leading publisher of Open Access books Built by scientists, for scientists

6,900

Open access books available

185,000

International authors and editors

200M

Downloads

Our authors are among the

154

Countries delivered to

TOP 1%

most cited scientists

12.2%

Contributors from top 500 universities



WEB OF SCIENCE™

Selection of our books indexed in the Book Citation Index
in Web of Science™ Core Collection (BKCI)

Interested in publishing with us?
Contact book.department@intechopen.com

Numbers displayed above are based on latest data collected.
For more information visit www.intechopen.com



Polarizability and Impurity Screening for Phosphorene

Po Hsin Shih, Thi Nga Do, Godfrey Gumbs
and Dipendra Dahal

Abstract

Using a tight-binding Hamiltonian for phosphorene, we have calculated the real part of the polarizability and the corresponding dielectric function, $\text{Re}[\epsilon(\mathbf{q}, \omega)]$, at absolute zero temperature ($T = 0$ K) with free carrier density $10^{13}/\text{cm}^2$. We present results showing $\text{Re}[\epsilon(\mathbf{q}, \omega)]$ in different directions of the transferred momentum q . When q is larger than a particular value which is twice the Fermi momentum k_F , $\text{Re}[\epsilon(\mathbf{q}, \omega)]$ becomes strongly dependent on the direction of \mathbf{q} . We also discuss the case at room temperature ($T = 300$ K). These results which are similar to those previously reported by other authors are then employed to determine the static shielding of an impurity in the vicinity of phosphorene.

Keywords: phosphorene, polarizability, impurity screening

1. Introduction

Emerging phenomena in physics and quantum information technology have relied extensively on the collective properties of low-dimensional materials such as two-dimensional (2D) and few-layer structures with nanoscale thickness. There, the Coulomb and/or atomic interactions play a crucial role in these complexes which include doped as well as undoped graphene [1–3], silicene [4, 5], phosphorene [6, 7], germanene [8, 9], antimonene [10, 11], tinene [12], bismuthene [13–18] and most recently the 2D pseudospin-1 $\alpha - T_3$ lattice [19]. Of these which have been successfully synthesized by various experimental techniques and which have been extensively investigated by various experimental techniques, few-layer black phosphorus (phosphorene) or BP has been produced by using mechanical cleavage [6, 20], liquid exfoliation [7, 21, 22], and mineralizer-assisted short-way transport reaction [23–25].

Unlike graphene, phosphorus inherently has an appreciable band gap. The observed photoluminescence peak of single-layer phosphorus in the visible optical range shows that its band gap is larger than that for bulk. Furthermore, BP has a middle energy gap (~ 1.5 – 2 eV) at the Γ point, thereby being quite different from the narrow or zero gaps of group-IV systems. Specifically, experimental measurements have shown that the BP-based field effect transistor has an on/off ratio of 105 and a carrier mobility at room temperature as large as $103 \text{ cm}^2/\text{Vs}$. We note that BP is expected to play an important role in the next-generation of electronic devices [6, 20]. Phosphorene exhibits a puckered structure related to the sp^3 hybridization of ($3s, 3p_x, 3p_y, 3p_z$) orbitals. The deformed hexagonal lattice of monolayer BP has four

atoms [26], while the group-IV honeycomb lattice includes two atoms. The low-lying energy dispersions, which are dominated by $3p_z$ orbitals, can be described by a four-band model with complicated multi-hopping integrals [26]. The low-lying energy bands are highly anisotropic, e.g., the linear and parabolic dispersions near the Fermi energy E_F , respectively, along the \hat{k}_x and \hat{k}_y directions. The anisotropic behaviors are further reflected in other physical properties, as verified by recent measurements on optical and excitonic spectra [27] as well as transport properties [6, 28].

In this work, we have examined the anisotropic behavior of the static polarizability and shielded potential of an impurity for BP. The calculations for the polarizability were executed at $T = 0$ K and room temperature ($T = 300$ K). We treat the buckled BP structure as a 2D sheet in our formalism. Consequently, we present an algebraic expression for the surface response function of a pair of 2D layers with arbitrary separation and which are embedded in dielectric media. We then adapt this result to the case when the layer separation is very small to model a free-standing buckled BP structure.

The outline of the rest of our presentation is as follows. In Section 2, we present the surface response function for a pair of 2D layers embedded in background dielectric media. We then simplify this result for a pair of planar sheets which are infinitesimally close to each other and use this for buckled BP. The tight-binding model Hamiltonian for BP is presented in Section 3. This is employed in our calculations of the energy bands and eigenfunctions. Section 4 is devoted to the calculation of the polarizability and dielectric function of BP showing its temperature dependence and their anisotropic properties as a consequence of its band structure. Impurity shielding by BP is discussed in Section 5 and we summarize our important results in Section 6.

2. Surface response function for a pair of 2D layers

Let us consider a heterostructure whose surface is in the xy -plane and suppose that r_{\parallel} denotes the corresponding in-plane translation vector. At time t , an external potential $\tilde{\phi}_{ext}(q, \omega)$ with wave vector q and frequency ω will give rise to an induced potential which, outside the structure, can be written as

$$\phi_{ind}(\mathbf{r}_{\parallel}, t) = - \int \frac{d^2 \mathbf{q}}{(2\pi)^2} \int_{-\infty}^{\infty} d\omega \tilde{\phi}_{ext}(q, \omega) e^{i(\mathbf{q} \cdot \mathbf{r}_{\parallel} - \omega t)} g(\mathbf{q}, \omega) e^{-qz}. \quad (1)$$

This equation defines the surface response function $g(\mathbf{q}, \omega)$. It has been implicitly assumed that the external potential ϕ_{ext} is so weak that the medium responds linearly to it.

The quantity $\text{Im}[g(\mathbf{q}, \omega)]$ can be identified with the power absorption in the structure due to electron excitation induced by the external potential. The total potential in the vicinity of the surface ($z \approx 0$), is given by

$$\phi(\mathbf{r}_{\parallel}, t) = \int \frac{d^2 \mathbf{q}}{(2\pi)^2} \int_{-\infty}^{\infty} d\omega (e^{qz} - g(\mathbf{q}, \omega) e^{-qz}) e^{i(\mathbf{q} \cdot \mathbf{r}_{\parallel} - \omega t)} \tilde{\phi}_{ext}(\mathbf{q}, \omega) \quad (2)$$

which takes account of nonlocal screening of the external potential.

2.1 Model for phosphorene layer

In this section, we present the surface response function we calculated for a structure which consists of a pair of 2D layers in contact with a dielectric medium,

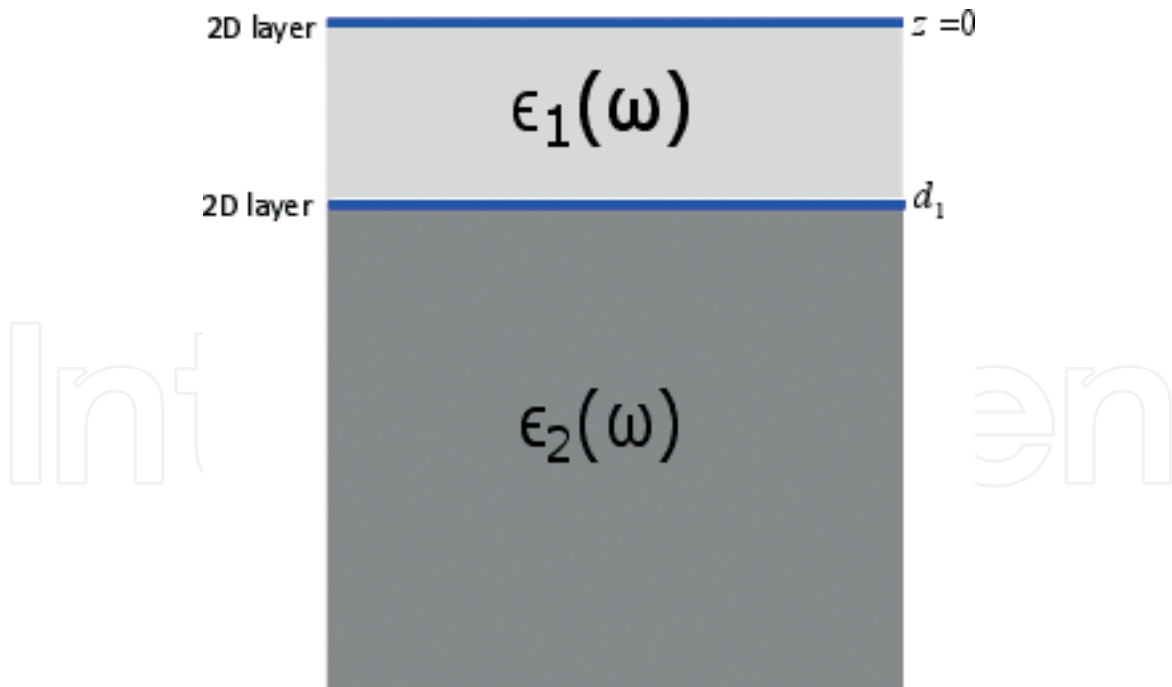


Figure 1.
 (Color online) Schematic illustration of a hybrid structure consisting of a pair of 2D layers separated by distance d_1 . The background materials are labeled by dielectric functions $\epsilon_1(\omega)$ and $\epsilon_2(\omega)$.

as shown in **Figure 1**. One of the 2D layers is at the top and the other is encapsulated by materials with dielectric constants $\epsilon_1(\omega)$, with thickness d_1 , and $\epsilon_2(\omega)$, of semi-infinite thickness. Calculation shows that the surface response function is given by [29, 30].

$$g(\mathbf{q}, \omega) = \frac{\mathcal{N}(\mathbf{q}, \omega)}{\mathcal{D}(\mathbf{q}, \omega)}, \quad (3)$$

where

$$\mathcal{N}(\mathbf{q}, \omega) \equiv e^{2d_1q} \{q\epsilon_0(\epsilon_1(\omega) - 1) - \chi_1(\mathbf{q}, \omega)\} \{q\epsilon_0(\epsilon_1(\omega) + \epsilon_2(\omega)) - \chi_2(\mathbf{q}, \omega)\} - \{q\epsilon_0(\epsilon_1(\omega) + 1) + \chi_1(\mathbf{q}, \omega)\} \{q\epsilon_0(\epsilon_1(\omega) - \epsilon_2(\omega)) + \chi_2(\mathbf{q}, \omega)\}, \quad (4)$$

and

$$\mathcal{D}(\mathbf{q}, \omega) \equiv e^{2d_1q} \{q\epsilon_0(\epsilon_1(\omega) + 1) - \chi_1(\mathbf{q}, \omega)\} \{q\epsilon_0(\epsilon_1(\omega) + \epsilon_2(\omega)) - \chi_2(\mathbf{q}, \omega)\} - \{q\epsilon_0(\epsilon_1(\omega) - 1) + \chi_1(\mathbf{q}, \omega)\} \{q\epsilon_0(\epsilon_1(\omega) - \epsilon_2(\omega)) + \chi_2(\mathbf{q}, \omega)\}. \quad (5)$$

In this notation, \mathbf{q} is the in-plane wave vector, ω is the frequency and $\chi_1(\mathbf{q}, \omega)$ and $\chi_2(\mathbf{q}, \omega)$ are the 2D layer susceptibilities.

When we take the limit $d_1 \rightarrow 0$, i.e., the separation between the two layers is small, the ϵ_1 drops out and we have the following result for the surface response function corresponding to the structure in **Figure 2**

$$g(\mathbf{q}, \omega) = 1 - \frac{1}{\frac{1+\epsilon_2(\omega)}{2} - \frac{\chi_1(\mathbf{q}, \omega) + \chi_2(\mathbf{q}, \omega)}{2q\epsilon_0}}. \quad (6)$$

Here, the dispersion equation which is given by the zeros of the denominator $\epsilon(\mathbf{q}, \omega)$ of the second term is expressed in terms of the ‘average’ susceptibility for the two layers. Clearly, this dispersion equation is that for a 2D layer of the Stern form where we make the identification $\chi \rightarrow e^2\Pi^{(0)}$ in terms of the polarizability. This

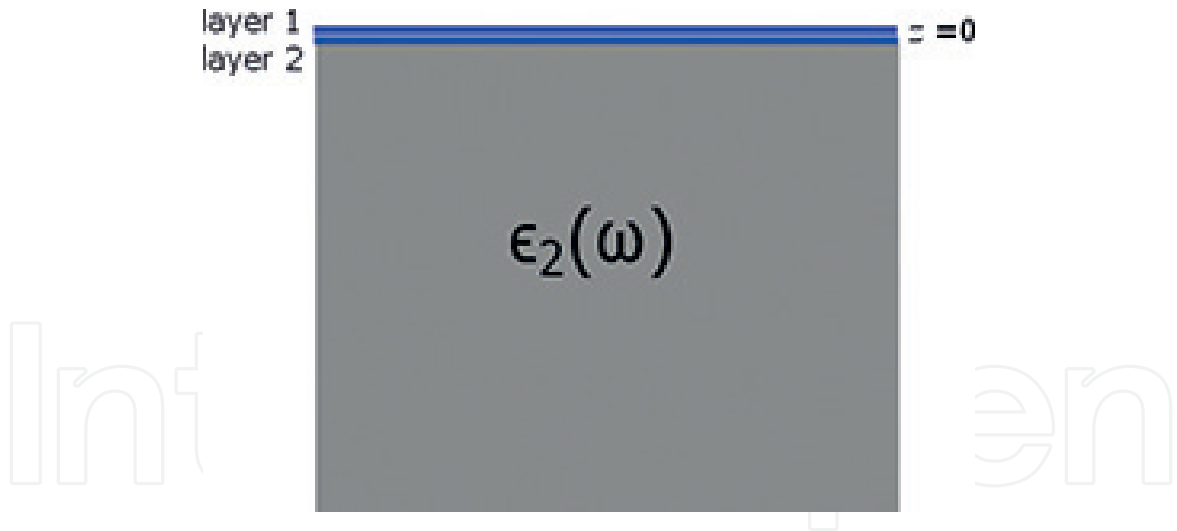


Figure 2.
(Color online) Schematic representation of a structure consisting of a pair of 2D layers which are infinitesimally close. There is vacuum above the layers and a dielectric below.

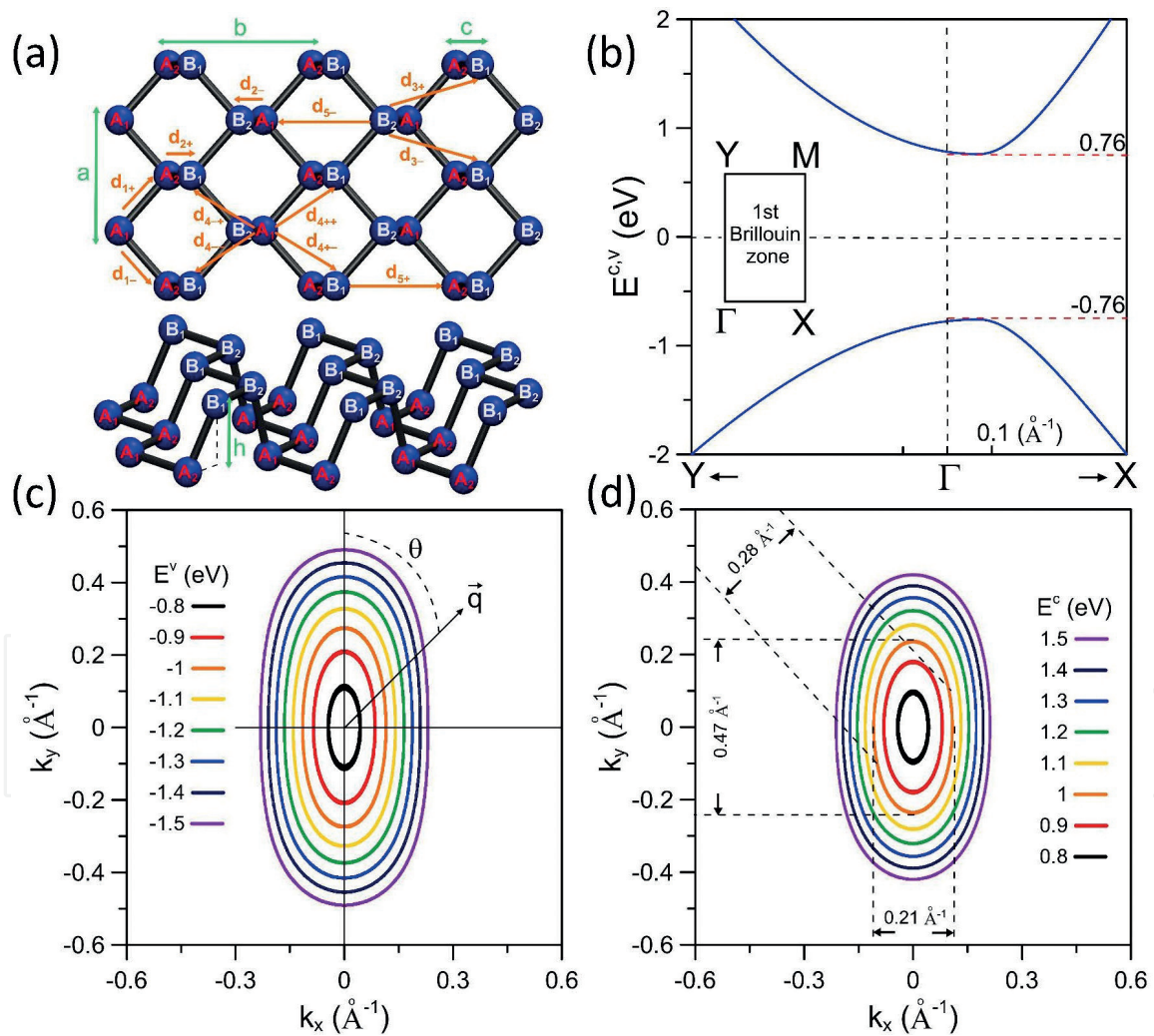


Figure 3.
(Color online) The (a) top view and side view of crystal structure for BP and (b) its band structure. The constant-energy diagrams are presented for (c) valence and (d) conduction bands. The values of $2 k_F$ for different θ are given in (d).

result in Eq. (6) clearly illustrates that for the buckled BP structure shown in **Figure 3**, the dielectric function can be treated as that for a single layer whose susceptibility arises from a combination of two rows of atoms making up the layer.

Our calculation can easily be generalized to the case when the monolayer is embedded above and below by the same thick dielectric material (dielectric constant ϵ_b) which corresponds to the free-standing situation which we consider below. For this, we have $\epsilon(\mathbf{q}, \omega) = \epsilon_b - e^2 / (2\epsilon_0 q) \Pi^{(0)}(\mathbf{q}, \omega)$, expressed in terms of the 2D layer polarizability $\Pi^{(0)}(\mathbf{q}, \omega)$.

3. Model Hamiltonian

Phosphorene is treated as a single layer of phosphorus atoms arranged in a puckered orthorhombic lattice, as shown in **Figure 3(a)**. It contains two atomic layers of A and B atoms and two kinds of bonds for in-plane and inter-plane P–P connections with different bond lengths. The low-lying electronic structure can be described by a tight-binding Hamiltonian, which is a 4×4 matrix within the basis (A_1, A_2, B_1, B_2) , of the form

$$\begin{bmatrix} 0 & T_1 + T_3^* & T_4 & T_{2-} + T_{5-}^* \\ T_1^* + T_3 & 0 & T_{2+} + T_{5+}^* & T_4 \\ T_4 & T_{2+}^* + T_{5+} & 0 & T_1 + T_3^* \\ T_{2-}^* + T_{5-} & T_4 & T_1^* + T_3 & 0 \end{bmatrix}.$$

Here, we consider up to five nearest atomic interactions through five independent terms of T_i with $i = 1, 2, 3, 4, 5$. These terms are given by the following expressions.

$$\begin{cases} T_1 = t_1 e^{i\mathbf{k} \cdot (\mathbf{d}_{1+} + \mathbf{d}_{1-})} \\ T_{2\pm} = t_2 e^{i\mathbf{k} \cdot \mathbf{d}_{2\pm}} \\ T_3 = t_3 e^{i\mathbf{k} \cdot (\mathbf{d}_{3+} + \mathbf{d}_{3-})} \\ T_4 = t_4 e^{i\mathbf{k} \cdot (\mathbf{d}_{4++} + \mathbf{d}_{4+-}^{\rightarrow} + \mathbf{d}_{4-+}^{\rightarrow} + \mathbf{d}_{4--})} \\ T_{5\pm} = t_5 e^{i\mathbf{k} \cdot \mathbf{d}_{5\pm}} \end{cases} \quad (7)$$

In this notation, t_m ($m = 1, 2, 3, 4, 5$) are the hopping integrals, corresponding to the atomic interactions. They have been optimized as ($t_1 = -1.220$, $t_2 = 3.665$, $t_3 = -0.205$, $t_4 = -0.105$, $t_5 = -0.055$) in order to reproduce the energy bands obtained by the density functional theory (DFT) calculations [31–33]. Also, $\vec{d}_{m\pm}$ are the vectors connecting the lattice sites which can be written as

$$\begin{cases} d_{1\pm} = (b/2 - c, \pm a/2, 0) \\ d_{2\pm} = (\pm c, 0, h) \\ d_{3\pm} = (b/2 + c, \pm a/2, 0) \\ d_{4\pm} = (\pm b/2, \pm a/2, h) \\ d_{5\pm} = \{\pm (b - c), 0, -h\}, \end{cases} \quad (8)$$

where $a = 3.314\text{\AA}$, $b = 4.376\text{\AA}$, $c = 0.705\text{\AA}$, and $h = 2.131\text{\AA}$ are the distances between the BP atoms [34, 35], as illustrated in **Figure 3(a)**.

The valence and conduction energy bands present strong anisotropic behaviors, as illustrated by the energy bands in **Figure 3(b)** and the constant-energy loops in **Figure 3(c)** and **(d)**. As a result, the polarizability and dielectric function are shown to be strongly dependent on the direction of the transferred momentum \mathbf{q} .

4. Dielectric function

When monolayer BP is perturbed by an external time-dependent Coulomb potential, all the valence and conduction electrons will screen this field and therefore create the charge redistribution. The effective potential between two charges is the sum of the external potential and the induced potential due to screening charges. The dynamical dielectric function, within the random-phase approximation (RPA), is given by [36].

$$\epsilon(\mathbf{q}, \omega) = \epsilon_b - V_q \sum_{s, s'=\alpha, \beta} \sum_{h, h'=\text{c}, v} \int_{1\text{stBZ}} \frac{dk_x dk_y}{(2\pi)^2} |\langle s'; h'; \mathbf{k} + \mathbf{q} | e^{i\mathbf{q}\cdot\mathbf{r}} | s; h; \mathbf{k} \rangle|^2 \times \frac{f(E^{s', h'}(\mathbf{k} + \mathbf{q})) - f(E^{s, h}(\mathbf{k}))}{E^{s', h'}(\mathbf{k} + \mathbf{q}) - E^{s, h}(\mathbf{k}) - (\omega + i\Gamma)}. \quad (9)$$

Here, the π -electronic excitations are described in terms of the transferred momentum \mathbf{q} and the excitation frequency ω . $\epsilon_b = 2.4$ the background dielectric constant, $V_q = 2\pi e^2/(\epsilon_s q)$ the 2D Fourier transform of the bare Coulomb potential energy ($\epsilon_s = 4\pi\epsilon_0$), and Γ the energy width due to various de-excitation mechanisms. $f(E) = 1/\{1 + \exp[(E - \mu)/k_B T]\}$ the Fermi-Dirac distribution in which k_B is the Boltzmann constant and μ the chemical potential corresponding to the highest occupied state energy (middle energy of band gap) in the (semiconducting) metallic systems at $T = 0$ K.

Figure 4(a) and **(b)** shows the directional/ θ -dependence of the static polarization function $\Pi^{(0)}(0, \mathbf{q})$, in which θ defines the angle between the direction of \mathbf{q} and the unit vector \hat{k}_y . For arbitrary θ , the polarization function at lower ($q \leq 0.2$ (1/Å))

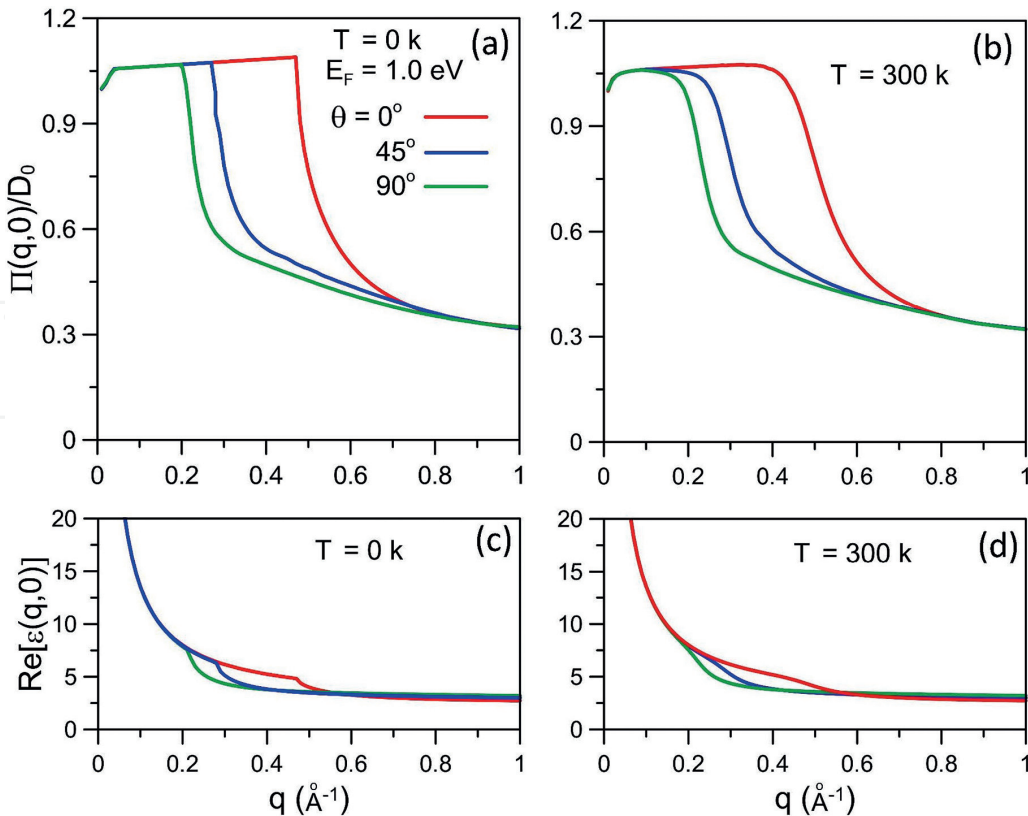


Figure 4.

(Color online) The static polarizability for BP as a function of wave vector for different directions of the transferred momentum \mathbf{q} at (a) absolute zero and (b) room temperatures. Plots (c) and (d) correspond to the static dielectric function of BP at $T = 0$ and 300 K, respectively.

and higher ($q \geq 0.7$ ($1/\text{\AA}$)) transferred momentum remains unchanged. In general, $\Pi^{(0)}(0, \mathbf{q})$ falls off rapidly beyond a critical value of q ($2k_F$) which depends on θ . For increasing θ from 0 to 90° , the specific values are getting larger, as shown in **Figure 4(a)**. This means that the polarizability is stronger for $0.2 \leq q \leq 0.7$ ($1/\text{\AA}$). The main features of the polarizability for BP are quite similar to those for the 2D electron gas, but different with those for graphene. Temperature has an effect on the polarization function which is demonstrated in **Figure 4(b)**. At room temperature, $\Pi^{(0)}(0, \mathbf{q})$ exhibits a shoulder-like structure near the critical values of q instead of step-like structure at $T = 0$.

Plots of the static dielectric function of BP for various values of θ are presented in **Figure 4(c)** and **(d)** at absolute zero and room temperatures, respectively. In the range of $0.2 \leq q \leq 0.5$ ($1/\text{\AA}$), there is a clear dependence of the dielectric function on the direction of the transferred momentum q . The $\text{Re } \epsilon(0, q)$ is higher with the growth of θ . The introduction of finite temperature smoothens the q -dependent $\text{Re } \epsilon(0, q)$, as shown in **Figure 4(d)** for $T = 30$ K.

5. Impurity shielding

Starting with Eq. (2), we obtain the static screening of the potential on the surface at $z = 0$ due to an impurity with charge Z_0^*e located at distance z_0 above the surface of BP as

$$\begin{aligned} \phi(\mathbf{r}_{\parallel}, \omega = 0) &= \frac{Z_0^*e}{2\pi\epsilon_0} \int_0^\infty dq \int_0^{2\pi} d\theta e^{iqr \cos\theta} [1 - g(\mathbf{q}, \omega = 0)] e^{-qz_0} \\ &= \frac{Z_0^*e}{2\pi\epsilon_0} \int_0^\infty dq \int_0^{2\pi} d\theta \frac{e^{iqr \cos\theta - qz_0}}{\epsilon(\mathbf{q}, \omega = 0)}. \end{aligned} \quad (10)$$

By employing the generalized form of Eq. (6) for free-standing BP in Eq. (10), we have computed the screened impurity potential. The screened potentials for various z_0 's are shown in **Figure 5** at absolute zero temperature and Fermi energy

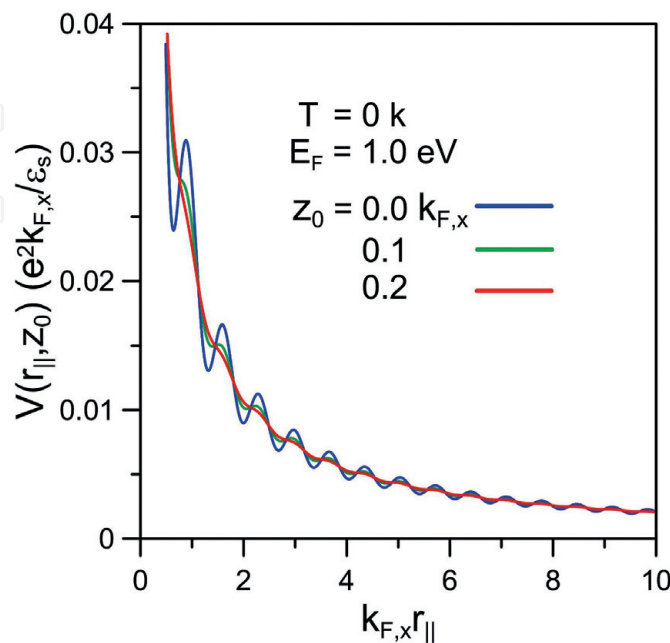


Figure 5.
 (Color online) The screened impurity potential in units of $e^2 k_{F,x} / (\epsilon_s)$ is plotted as a function of $k_{F,x} r_{\parallel}$ for the chosen parameters in the figure.

$E_F = 1.0$ eV. There exist Friedel oscillations for sufficiently small z_0 . Such oscillations might be smeared out for larger z_0 , e.g., the green and red curves. It is noticed that for $E_F = 1.0$ eV, the room temperature of 300 K which is much smaller than the Fermi temperature (10,000 K) does not have significant effect on the screened potential. Apparently, $V(r_{\parallel}, z_0)$ at $T = 0$ and 300 K (not shown) are almost equivalent.

6. Concluding remarks and summary

The energy band structure of BP, calculated using the tight-binding method, is anisotropic and so are its polarizability, dielectric function and screened potential. To illustrate these facts, we have presented numerical results for the polarizability in the x and y directions for a range of doping concentrations. The $\text{Re}[\epsilon(\mathbf{q}, \omega = 0)]$ of the static dielectric function for BP also reveals some interesting characteristics. At absolute zero temperature ($T = 0$) and with free carrier density corresponding to chosen Fermi energy E_F , we have presented numerical results for $\text{Re}[\epsilon(\mathbf{q}, \omega = 0)]$ in different directions of the transferred momentum \mathbf{q} . When q is larger than a critical value which is twice the Fermi momentum k_F , our calculations show that $\text{Re}[\epsilon(\mathbf{q}, \omega = 0)]$ becomes substantially dependent on the direction of \mathbf{q} . We also discuss the case at room temperature ($T = 300$ K). These results are in agreement with those reported by other authors. We employ our data to determine the static shielding of an impurity in the vicinity of phosphorene.

Acknowledgements

G.G. would like to acknowledge the support from the Air Force Research Laboratory (AFRL) through Grant #12530960.

Conflict of interest

All the authors declare that they have no conflict of interest.

IntechOpen

Author details

Po Hsin Shih¹, Thi Nga Do², Godfrey Gumbs^{3,4*} and Dipendra Dahal³

¹ Department of Physics, National Cheng Kung University, Tainan, Taiwan

² Institute of Physics, Academia Sinica, Taipei, Taiwan

³ Department of Physics and Astronomy, Hunter College of the City University of New York, New York, NY, USA

⁴ Donostia International Physics Center (DIPC), San Sebastian, Basque Country, Spain

*Address all correspondence to: ggumbs@hunter.cuny.edu

IntechOpen

© 2018 The Author(s). Licensee IntechOpen. This chapter is distributed under the terms of the Creative Commons Attribution License (<http://creativecommons.org/licenses/by/3.0>), which permits unrestricted use, distribution, and reproduction in any medium, provided the original work is properly cited. 

References

- [1] Novoselov KS, Geim AK, Morozov SV, Jiang D, Zhang Y, Dubonos SV, et al. Electric field effect in atomically thin carbon films. *Science*. 2004;**306**:666-669. DOI: 10.1126/science.1102896
- [2] Dbbelin M, Ciesielski A, Haar S, Osella S, Bruna M, Minoia A, et al. Light-enhanced liquid-phase exfoliation and current photoswitching in graphene-azobenzene composites. *Nature Communications*. 2016;**7**:11090. DOI: 10.1038/ncomms11090
- [3] Kim KS, Zhao Y, Jang H, Lee SY, Kim JM, Kim KS, et al. Large-scale pattern growth of graphene films for stretchable transparent electrodes. *Nature*. 2009;**457**:706-710. DOI: 10.1038/nature07719
- [4] Tao L, Cinquanta E, Chiappe D, Grazianetti C, Fanciulli M, Dubey M, et al. Silicene field-effect transistors operating at room temperature. *Nature Nanotechnology*. 2015;**10**:227-231. DOI: 10.1038/nnano.2014.325
- [5] Vogt P, De Padova P, Quaresima C, Avila J, Frantzeskakis E, Asensio MC, et al. Silicene: Compelling experimental evidence for Graphenelike two-dimensional silicon. *Physical Review Letters*. 2012;**108**:155501. DOI: 10.1103/PhysRevLett.108.155501
- [6] Li L, Yu Y, Ye GJ, Ge Q, Ou X, Wu H, et al. Black phosphorus field-effect transistors. *Nature Nanotechnology*. 2014;**9**:372-377. DOI: 10.1038/nnano.2014.35
- [7] Yasaei P, Kumar B, Foroozan T, Wang C, Asadi M, Tuschel D, et al. High-quality black phosphorus atomic layers by liquid-phase exfoliation. *Advanced Materials*. 2015;**27**:1887-1892. DOI: 10.1002/adma.201405150
- [8] Li L, Lu S, Pan J, Qin Z, Wang Y, Wang Y, et al. Buckled Germanene formation on Pt(111). *Advanced Materials*. 2014;**26**:4820-4824. DOI: 10.1002/adma.201400909
- [9] Derivaz M, Dentel D, Stephan R, Hanf M-C, Mehdaoui A, Sonnet P, et al. Continuous Germanene layer on Al (111). *Nano Letters*. 2015;**15**:2510-2516. DOI: 10.1021/acs.nanolett.5b00085
- [10] Ji J, Song X, Liu J, Yan Z, Huo C, Zhang S, et al. Two-dimensional antimonene single crystals grown by van der Waals epitaxy. *Nature Communications*. 2016;**7**:13352. DOI: 10.1038/ncomms13352
- [11] Ares P, Aguilar Galindo F, Rodríguez San Miguel D, Aldave DA, Díaz Tendero S, Alcamí M, et al. Antimonene: Mechanical isolation of highly stable antimonene under ambient conditions. *Advanced Materials*. 2016;**28**:6515-6515. DOI: 10.1002/adma.201670209
- [12] Zhu F, Chen W, Xu Y, Gao C, Guan D, Liu C, et al. Epitaxial growth of two-dimensional stanene. *Nature Materials*. 2015;**14**:1020-1025. DOI: 10.1038/nmat4384
- [13] Hirahara T, Nagao T, Matsuda I, Bihlmayer G, Chulkov EV, Koroteev YM, et al. Role of spin-orbit coupling and hybridization effects in the electronic structure of ultrathin Bi films. *Physical Review Letters*. 2006;**97**:146803. DOI: 10.1103/PhysRevLett.97.146803
- [14] Hirahara T, Shirai T, Hajiri T, Matsunami M, Tanaka K, Kimura S, et al. Role of quantum and surface-state effects in the bulk Fermi-level position of ultrathin Bi films. *Physical Review Letters*. 2015;**115**:106803. DOI: 10.1103/PhysRevLett.115.106803
- [15] Hirahara T, Fukui N, Shirasawa T, Yamada M, Aitani M, Miyazaki H, et al.

Atomic and electronic structure of ultrathin Bi(111) films grown on Bi₂Te₃(111) substrates: Evidence for a strain-induced topological phase transition. *Physical Review Letters*. 2012;**109**:227401. DOI: 10.1103/PhysRevLett.109.227401

[16] Yang F, Miao L, Wang ZF, Yao M-Y, Zhu F, Song YR, et al. Spatial and energy distribution of topological edge states in single Bi(111) bilayer. *Physical Review Letters*. 2012;**109**:016801. DOI: 10.1103/PhysRevLett.109.016801

[17] Wang ZF, Yao M-Y, Ming W, Miao L, Zhu F, Liu C, et al. Creation of helical Dirac fermions by interfacing two gapped systems of ordinary fermions. *Nature Communications*. 2013;**4**:1384. DOI: 10.1038/ncomms2387

[18] Sabater C, Gosálbez-Martínez D, Fernández-Rossier J, Rodrigo JG, Untiedt C, Palacios JJ. Topologically protected quantum transport in locally exfoliated bismuth at room temperature. *Physical Review Letters*. 2013;**110**:176802. DOI: 10.1103/PhysRevLett.110.176802

[19] Malcolm JD, Nicol EJ. Frequency-dependent polarizability, plasmons, and screening in the two-dimensional pseudospin-1 dice lattice. *Physical Review B*. 2016;**93**:165433. DOI: 10.1103/PhysRevB.93.165433

[20] Liu H, Neal AT, Zhu Z, Luo Z, Xu X, Tomnek D, et al. Phosphorene: An unexplored 2D semi-conductor with a high hole mobility. *ACS Nano*. 2014;**8**:4033-4041. DOI: 10.1021/nn501226z

[21] Brent JR, Savjani N, Lewis EA, Haigh SJ, Lewis DJ, O'Brien P. Production of few-layer phosphorene by liquid exfoliation of black phosphorus. *Chemical Communications*. 2014;**50**:13338-13341. DOI: 10.1039/C4CC05752J

[22] Kang J, Wood JD, Wells SA, Lee J-H, Liu X, Chen K-S, et al. Solvent exfoliation

of electronic-grade, two-dimensional black phosphorus. *ACS Nano*. 2015;**9**:3596-3604. DOI: 10.1021/acsnano.5b01143

[23] Lange S, Schmidt P, Nilges T. Au₃SnP₇@black phosphorus: An easy access to black phosphorus. *Inorganic Chemistry*. 2007;**46**:4028-4035. DOI: 10.1021/ic062192q

[24] Nilges T, Kersting M, Pfeifer T. A fast low-pressure transport route to large black phosphorus single crystals. *Journal of Solid State Chemistry*. 2008;**181**:1707-1711. DOI: 10.1016/j.jssc.2008.03.008

[25] Köpf M, Eckstein N, Pfister D, Grotz C, Krüger I, Greiwe M, et al. Access and in situ growth of phosphorene-precursor black phosphorus. *Journal of Crystal Growth*. 2014;**405**:6-10. DOI: 10.1016/j.jcrysgr.2014.07.029

[26] Rudenko AN, Katsnelson MI. Quasiparticle band structure and tight-binding model for single- and bilayer black phosphorus. *Physical Review B*. 2014;**89**:201408. DOI: 10.1103/PhysRevB.89.201408

[27] Berman OL, Gumbs G, Kezerashvili RY. Bose-Einstein condensation and superfluidity of dipolar excitons in a phosphorene double layer. *Physical Review B*. 2017;**96**:014505. DOI: 10.1103/PhysRevB.96.014505

[28] Low T, Rodin AS, Carvalho A, Jiang Y, Wang H, Xia F, et al. Tunable optical properties of multilayer black phosphorus thin films. *Physical Review B*. 2014;**90**:075434. DOI: 10.1103/PhysRevB.90.075434

[29] Gumbs G, Huang D. *Properties of Interacting Low-Dimensional Systems*. 1st ed. New York: Wiley; 2011. 113 p. DOI: 10.1002/9783527638154

[30] Dahal D, Gumbs G, Huang D. Effect of strain on plasmons, screening, and

energy loss in graphene/substrate contacts. *Physical Review B*. 2018;**98**:045427. DOI: 10.1103/PhysRevB.98.045427

[31] Heyd J, Scuseria GE, Ernzerhof M. Hybrid functionals based on a screened Coulomb potential. *The Journal of Chemical Physics*. 2003;**118**:8207-8215. DOI: 10.1063/1.1564060

[32] Heyd J, Scuseria GE, Ernzerhof M. Erratum. Hybrid functionals based on a screened Coulomb potential. *The Journal of Chemical Physics*. 2006;**124**:219906. DOI: 10.1063/1.2204597

[33] Pez CJ, DeLello K, Le D, Pereira ALC, Mucciolo ER. Disorder effect on the anisotropic resistivity of phosphorene determined by a tight-binding model. *Physical Review B*. 2016;**94**:165419. DOI: 10.1103/PhysRevB.94.165419

[34] Takao Y, Asahina H, Morita A. Electronic structure of black phosphorus in tight binding approach. *Journal of the Physical Society of Japan*. 1981;**50**:3362-3369. DOI: 10.1143/JPSJ.50.3362

[35] Osada T. Edge state and intrinsic hole doping in bilayer phosphorene. *Journal of the Physical Society of Japan*. 2014;**84**:013703. DOI: 10.7566/JPSJ.84.013703

[36] Shung KW-K. Dielectric function and plasmon structure of stage-1 intercalated graphite. *Physical Review B*. 1986;**34**:979-993. DOI: 10.1103/PhysRevB.34.979